RSC Advances

PAPER

View Article Online
View Journal | View Issue

Cite this: *RSC Adv.*, 2025, **15**, 15893

Cellulose nanocrystal-supported silver nanoparticles as an antibacterial additive for PVA and PLLA matrices in meat packaging†

Mohamed Aouay, *[a] Anissa Haddar, *[bc] Emna Sellami,[b] Albert Magnin,[d] Jean-Luc Putaux [e] and Sami Boufi[a]

This study explored the synergistic potential of periodate-oxidized cellulose nanocrystals (CNCs) decorated with silver nanoparticles (AgNPs) to enhance the antimicrobial and mechanical properties of poly(vinyl alcohol) (PVA) and poly(L-lactic acid) (PLLA) biopolymer matrices. A concentration-dependent antibacterial activity was demonstrated against both Gram+ and Gram− bacteria, highlighting the potential of CNCs-AgNPs in inhibiting pathogenic strains. Moreover, the tensile strength of PVA and PLLA films was notably improved by incorporating CNCs-AgNPs. The filler demonstrated significant inhibitory effects on bacterial growth in chicken meat samples wrapped in PVA/CNCs-AgNPs nanocomposite films, allowing for an extension of the meat shelf life beyond acceptable microbiological limits. These results highlight the versatile capabilities of CNCs-AgNPs in polymer nanocomposites, positioning them as potent agents for antimicrobial packaging and as contenders for sustainable and functional nanomaterials in various applications.

Received 28th February 2025
Accepted 5th May 2025

DOI: 10.1039/d5ra01457c

rsc.li/rsc-advances

1 Introduction

As the demand for renewable sources continues to rise, the need for ecofriendly and biodegradable materials has become a top priority. In response, there has been a significant increase in the development and commercialization of biobased products. One such product is nanocellulose (NC) which has gained increasing attention due to its unique properties and potential applications in various fields. Its advantages over traditional materials include high strength, lack of toxicity, biodegradability, and biocompatibility.[1–4]

Immobilizing other functional materials, such as metal nanoparticles (M-NPs), onto the surface of NCs potentially enhances performance and expands their range of applications. Cellulose nanocrystals (CNCs) possess the required characteristics as chemically reactive biotemplates for M-NP synthesis.[5,6] Various methods, including chemical reduction, physical adsorption, and electrostatic interactions, have been used to attach M-NPs onto the surface of NC.[7,8] In this context, CNCs have been extensively used due to their high surface area, high aspect ratio, and abundant surface hydroxyl groups that enable surface modifications to introduce various functional groups, such as carboxyl, amino, or sulfonic acid groups. This modification facilitates the adsorption and reduction of metal ions, promoting the formation of M-NPs.[9] CNCs have been used as a template or stabilizing agent for synthesizing particles of various metals, including gold (Au), silver (Ag), copper (Cu), platinum (Pt), palladium (Pd), and zinc oxide (ZnO).[10–13] The resulting CNCs/M-NPs composites possess unique antimicrobial, optical, electronic, and catalytic properties that are useful for various applications, including packaging, biosensors, drug delivery, catalysis, and photonics.[10,12,14]

Silver is widely recognized for its exceptional antibacterial properties. Advancements in nanotechnology have further enhanced its effectiveness by introducing unique nanoscale features, such as high surface reactivity, large specific surface area, and strong bactericidal activity. However, studies have shown that free Ag nanoparticles (AgNPs) could accumulate within cells, causing a toxicity that restricts their use in food packaging materials.[15] To address this issue, researchers have immobilized AgNPs in films of chemically modified NC,[16] which significantly reduced the release of AgNPs, thereby decreasing their cytotoxicity and making them safer for practical applications.

In particular, CNCs decorated with AgNPs (CNCs-AgNPs) are promising candidates for enhancing the antimicrobial properties of nanocomposites. CNCs have been proposed to act both as a reducing agent for the synthesis of AgNPs and as a substrate for the immobilization of AgNPs, thereby enhancing

[a]University of Sfax, LMSE, Faculty of Science, BP 802, 3018 Sfax, Tunisia. E-mail: med_aouay@hotmail.fr

[b]University of Sfax, Laboratory for the Improvement of Plants and Valorization of Agroresources, ENIS, 3038 Sfax, Tunisia

[c]University of Sfax, High Institute of Biotechnology, Sfax, Tunisia. E-mail: anissa.haddar@isbs.usf.tn

[d]Univ. Grenoble Alpes, CNRS, Grenoble INP, LRP, F-38000 Grenoble, France

[e]Univ. Grenoble Alpes, CNRS, CERMAV, F-38000 Grenoble, France

† Electronic supplementary information (ESI) available. See DOI: https://doi.org/10.1039/d5ra01457c

antimicrobial activity.[17,18] The combination of CNCs with AgNPs provides a unique opportunity to create materials with improved antimicrobial properties while utilizing renewable, ecofriendly, and biodegradable materials.

Different approaches have been described for synthesizing CNCs-AgNPs and evaluating their efficacy in bacterial growth prevention. Shi *et al.* reported a bioinspired coating strategy for stabilizing unstable AgNPs using CNCs modified with dopamine. The hybrid NPs exhibited excellent colloidal stability and enhanced antibacterial activity against *Escherichia coli* and *Bacillus subtilis,* showing a more than fourfold increase compared to AgNPs alone.[19] New CNC and CNCs-AgNPs formulations have improved the water/air barrier properties and antibacterial characteristics of papers as well as their mechanical properties. At a 7 wt, CNCs-AgNPs increased tensile strength (T_s), decreased water vapor permeability (WVP) and air permeability, and exhibited higher antibacterial effects against *E. coli* and *S. aureus.*[20] Green nanocomposites were synthesized using poly(3-hydroxybutyrate-*co*-3-hydroxyvalerate) (PHBV) and CNCs-AgNPs as bifunctional reinforcements, resulting in improved thermal, mechanical, and antibacterial properties. Nanocomposites with 10 wt% CNCs-AgNPs showed a 140% increase in T_s compared to pristine PHBV, as well as lower water uptake, WVP, and migration levels, with strong antibacterial activity.[21] In another study, nanocomposites were developed from carboxylated CNCs and AgNPs to enhance the mechanical and antimicrobial properties of waterborne polyurethane (WPU).[22] In a previous article, we described the functionalization of cellulose nanofibrils (CNFs) and used Tollens' reagent to reduce Ag ions to AgNPs that nucleated, grew, and remained strongly attached to the CNFs. The resulting hybrid nanofibrils exhibited effective bactericidal properties against Gram+ and Gram− bacteria, without compromising the reinforcing potential of CNFs.[23]

Packaging is crucial for fresh and processed food products as a protective barrier against external contaminants, gas composition, spoilage bacteria, mechanical loads, and physical damage.[24] The introduction of CNCs-AgNPs significantly enhanced the mechanical and barrier properties of poly(L-lactic acid) (PLLA),[25–27] PHBV,[28] and poly(vinyl alcohol) (PVA),[29] three polymers widely used in packaging applications. Among these polymers, fully hydrolyzed PVA is commonly used as a coating layer in polymer- and paper-based packaging due to its excellent oxygen barrier properties.[30] Unlike its partially hydrolyzed counterpart, fully hydrolyzed PVA remains insoluble in water up to 50 °C, making it particularly suitable for applications requiring moisture resistance.[31] On the other hand, PLLA is a biobased and biodegradable (under specific conditions) polyester that gained significant attention for its potential use in various packaging formats, including films, bottles, and food containers.[32] Due to its good mechanical strength and transparency, PLLA is a promising alternative to conventional petrosourced plastics.

Combining CNCs-AgNPs with such biodegradable polymers is an emerging approach to developing high-performance, sustainable packaging materials with enhanced antibacterial and barrier properties. Yalcinkaya *et al.* prepared composite PLLA films by cast-drying incorporating AgNPs grafted onto CNCs.[33] Notably, the composite film containing 0.5 wt% AgNPs demonstrated 89% antibacterial activity against *E. coli* after an incubation period of 6 h. The results agreed with the findings of Hajji *et al.* who demonstrated the antibacterial activity of chitosan–PVA films.[34] In a similar vein, Ma *et al.* reported the high antibacterial activity of the PLA/poly(butylene adipate-*co*-terephthalate)/CNCs-AgNPs nanocomposites in killing both Gram− *E. coli* and Gram+ *S. aureus*,[35] while Fan *et al.* noted the substantial antibacterial properties of PVA/CNC-AgNPs nanocomposite films against both *S. aureus* and *E. coli.*[36] Sarwar *et al.* reported a notable bactericidal effect of PVA films containing CNCs and AgNPs added separately, demonstrating their efficacy against both *S. aureus* and *E. coli*.[37]

Despite advancements in the development of CNCs-AgNPs, achieving a sustainable and efficient synthesis route that meets industrial scalability and safety standards remains a challenge. This study aimed at (i) preparing and characterizing periodate-oxidized CNCs (ox-CNCs) as reducing agents for AgNP synthesis using Tollens' reagent, and (ii) evaluating the antibacterial properties of PVA and PLLA films incorporating CNCs-AgNPs against both Gram+ and Gram− bacteria. The process used to convert Ag ions to Ag^0 nuclei that subsequently clustered on the ox-CNC surface, forming metallic AgNPs, is described in Scheme 1. The reduction proceeded *via* electron transfer from the aldehyde groups present on the ox-CNC surface acting as reducing agent to the $[Ag(NH_3)_2]^+$ precursor. The fact that the reduction sites were located on the CNC surface was expected to ensure that AgNPs remained intimately bound to cellulose. The resulting CNCs-AgNPs were incorporated into PLLA *via* solvent-free melt extrusion, and into PVA by water-based solvent casting. Overall, this protocol supported sustainability by (i) utilizing the renewable nature and commercial availability of CNCs, (ii) avoiding harsh reducing agents, and (iii) employing scalable environmentally friendly preparation techniques.

2 Materials and methods

2.1. Materials

A commercially available CNC powder was purchased from Celluforce (Montreal, Canada). Sodium metaperiodate ($NaIO_4$), silver nitrate ($AgNO_3$, 99.9%), sodium hydroxide (NaOH), ammonium hydroxide (NH_3OH, 25%), and poly(ethylene glycol) (PEG, 35,000 g mol^{-1}) were purchased from Sigma-Aldrich. The nanocomposite films were prepared using commercial PLLA in pellet form (PLE 005-France) supplied by NaturePlast, and PVA (hydrolysis degree 98%) from Sigma-Aldrich.

2.2. Synthesis of CNCs-AgNPs

CNCs-AgNPs were prepared according to a three-step process (Scheme 1):

(i) Preparation of oxidized CNCs (ox-CNCs): in a 250 mL round bottom flask, 100 mL of deionized water was added to the CNC powder (1 g). $NaIO_4$ (3.27 mmol) was added and the resulting mixture was stirred in the dark for 48 h at 40 °C. The

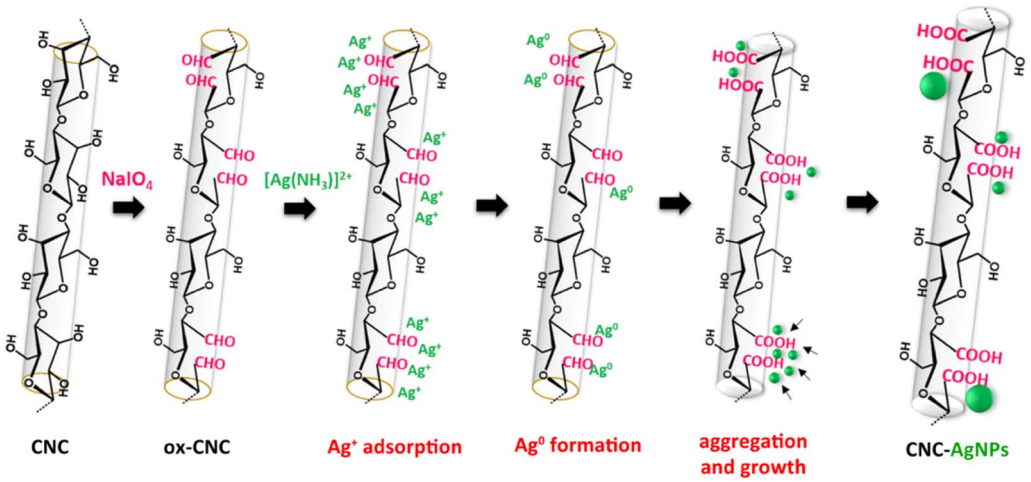

Scheme 1 Strategy to nucleate and grow AgNPs onto periodate-oxidized CNCs and Tollens' reaction. The green particles are newly formed AgNPs.

ox-CNCs were collected by centrifugation and thoroughly washed with deionized water to remove residual ionic species. This process was repeated three times to ensure the complete removal of ionic contaminants.

(ii) Preparation of Tollens' reagent: a 0.1 M solution of silver nitrate and a 0.1 M NaOH solution were prepared separately and then mixed, resulting in the precipitation of a brown Ag_2O powder. To dissolve Ag_2O, a 2 wt% aqueous ammonium solution was added dropwise to the mixture under magnetic stirring. As the ammonium solution was added, the brown powder gradually disappeared, promoting the formation of $[Ag(NH_3)_2]^+$.

(iii) Preparation of CNCs-AgNPs: ox-CNCs (1 g) were suspended in 100 mL water and heated at 45 °C for 1 h. 5.6 mL of 0.1 M Tollens' reagent was added to a concentration of 5×10^{-3} M $[Ag(NH_3)_2]^+$, and the mixture was magnetically stirred for 1 h. Immediately after addition of Tollens' reagent, the CNC suspension turned dark brown and was centrifuged at 5000 rpm for 15 min. The pellet was recovered, redispersed in water, and centrifuged three times to remove remaining salts. Finally, the suspension was dialyzed against distilled water to remove residual $Ag(NH_3)_2$ or Ag^+, which was verified by testing the neutrality of the dialysis effluent.

2.3. Particle size and ζ-potential measurements

The CNCs-AgNPs suspension was diluted to approximately 0.1 wt% with distilled water and analyzed at 25 °C using a Malvern Nano ZS Zetasizer instrument. The particle size was reported as the Z-average mean diameter, representing the diameter of an equivalent hard sphere that exhibits the same diffusion coefficient as the measured particle. For ζ-potential measurements, the sample concentration was adjusted to 0.01% wt% in water. Each measurement was conducted in triplicates, and the results were averaged.

2.4. Particle morphology

A droplet of CNCs-AgNPs suspension was deposited on a carbon-coated copper grid, stained with 2 wt% uranyl acetate, and allowed to air dry. The samples were observed with a JEOL JEM-2100 Plus transmission electron microscope (TEM) operating at 200 kV and images were recorded using a Gatan Rio 16 digital camera. The particle size was measured using the ImageJ software (version 1.53e).

2.5. Nanocomposite processing

2.5.1. PLLA/CNCs-AgNPs composites. CNCs-AgNPs were sonicated for 2 min at 70% amplitude, mixed with PEG in a DSM-Xplore15cc microcompounder at 195 °C and 120 rpm, and oven-dried for 48 h. The resulting blends were dried at 45 °C for 24 h and manually milled into small particles. The nanocomposite films were finally extruded by feeding PLLA and CNCs-AgNPs/PEG pellets into the extruder equipped with a flat sheet die with a 3×0.15 mm^2 rectangular cross-section. Three PLLA-PEG-CNC formulations were tested, noted 95-5-0, 93-5-2, and 91-5-4 (in wt%), respectively.

2.5.2. PVA/CNCs-AgNPs composites. Dry PVA granules were first dissolved in deionized water at 90 °C at 15 wt% solid content. CNCs-AgNPs were sonicated for 1 min to ensure proper dispersion and added to the PVA solution at a concentration ranging from 0 to 4 wt%. The mixture was stirred for 1 h at room temperature to produce a homogeneous blend that was dry cast in a Petri dish for 24 h at 40 °C to form a nanocomposite film.

2.6. Thermal stability

The thermal stability of Ox-CNCs and CNCs-AgNPs was evaluated by thermogravimetric analysis (TGA) with a PerkinElmer TGA 400 analyzer. The measurements were conducted under an airflow, heating the samples from 30 to 750 °C at a rate of 10 °C min^{-1}.

2.7. Mechanical properties

Specimen were cut to 20 mm × 40 mm strips and a thickness of *ca.* 100 μm. Tensile tests were performed according to the ASTM D638 standard, using an Instron machine equipped with a 100 N load cell. The tests were carried out at 25 °C and 40%

relative humidity (RH), with a cross-head speed of 10 mm min^{-1}. Five specimens per sample were tested and the results were reported as average values accompanied by standard deviations.

2.8. X-ray diffraction (XRD)

Film strips were attached to a metallic collimator and analyzed in transmission mode with an X-ray beam produced by a Philips PW3830 generator (30 kV, 20 mA, CuKα radiation, $\lambda = 0.1542$ nm). Two-dimensional diffraction patterns were recorded on Fujifilm imaging plates read with a Fujifilm BAS 1800-II bio-analyzer, and rotationally averaged to produce diffraction profiles.

2.9. UV-vis spectroscopy

Absorption spectra ranging from 200 to 800 nm were collected with a Lambda 35UV visible spectrometer from PerkinElmer.

2.10. Antibacterial properties of CNCs-AgNPs

Culture suspensions (100 μL) containing Gram– bacteria (*Escherichia coli* (ATCC 25922), *Klebsiella pneumoniae* (ATCC 13883), *Salmonella enterica* (ATCC 43972), *Pseudomonas aeruginosa* (ATCC 27853) and Gram+ bacteria (*Staphylococcus aureus* (ATCC 25923), *Micrococcus luteus* (ATCC 4698), *Listeria monocytogenes* (ATCC 43251), *Enterococcus faecalis* (ATCC 29212) at a concentration of 10^6 colony-forming units (CFU mL^{-1}) were spread on Luria–Bertani (LB) agar. Wells with a diameter of 5 mm were punched into the agar, and 1, 2, and 4 wt% CNCs-AgNPs were loaded into the wells. The agar plates were refrigerated at 4 °C for 1 h before being incubated at 37 °C for 24 h. The antibacterial activity was assessed by measuring the diameter of the growth inhibition regions (expressed in millimeters) around the wells. The impact of CNCs-AgNPs on bacterial growth in liquid broth was investigated as well. Bacterial cultures in the log phase in LB medium were incubated at 37 °C at 150 rpm, after adding CNCs-AgNPs at 0.1, 0.2, 0.4, 0.8, 1.6, and 3.2 mg mL^{-1}. Control broths without nanoparticles were also tested. After an 18 h incubation at 37 °C, a serial dilution from each sample containing culture and the controls was performed. The microbial inhibition was determined by counting the colony-forming units (CFU) by inoculating Petri dishes containing solidified nutrient agar medium with 100 μL from each dilution and calculating the number of appearing colonies compared to the controls.

2.11. Determination of minimum inhibitory concentration

The minimum inhibitory concentration (MIC) of CNCs-AgNPs was established using a liquid growth inhibition assay conducted in microtiter plate wells, following the method described by Andrews.[38] The MIC is defined as the lowest concentration of CNCs-AgNPs that completely inhibits the growth of the tested strain. Bacterial strains were subjected to serial dilutions of CNCs-AgNPs from 6.4 to 0.1 mg mL^{-1} and incubated at 37 °C for 24 h.

2.12. Antibacterial properties of PVA and PLA nanocomposite films incorporating CNCs-AgNPs

The antibacterial effectiveness of PVA/CNCs-AgNPs and PLLA/CNCs-AgNPs films was evaluated using the agar diffusion method and the following bacterial strains: *E. coli* (ATCC 25922), *K pneumoniae* (ATCC 13883), *S. enterica* (ATCC 43972), *P. aeruginosa* (ATCC 27853), *S. aureus* (ATCC 25923), *M. luteus* (ATCC 4698), *L. monocytogenes* (ATCC 43251), and *E. faecalis* (ATCC 29212). The bacteria were initially cultured in a flask with 9 mL of LB. Aliquots of each culture suspension (100 μL at 10^6 CFU mL^{-1}) were used for antibacterial assays. The nanocomposite films (1 cm × 1 cm) were subjected to UV-light sterilization for 10 min before being placed on agar plates and incubated for 24 h at 37 °C. The antibacterial activity was determined by the development of an inhibition region beneath or around the film. Films of neat PVA and PLLA were used as controls.

2.13. Application of PVA/CNCs-AgNPs films for chicken breast fillet packaging

Fresh chicken breast fillet samples, purchased from a local supermarket in Sfax (Tunisia), underwent aseptic preparation into 25 g square pieces that were wrapped in PVA/CNCs-AgNPs 70 mm × 70 mm films. In addition, a control chicken breast fillet was wrapped in a neat PVA film of the same size. All chicken meat samples were stored for 7 days at 4 °C and analyzed on days 1, 3, 5, and 7.

2.14. Microbiological analyses of chicken breast fillets during storage

Microbiological examinations were conducted on the entirety of chicken breast fillets. A sterile stomacher filter bag contained 25 g of chicken fillets, to which 225 mL of sterile peptone-water solution was aseptically added. The mixture was homogenized for 3 min using a BA6021 stomacher 400. Serial dilutions were prepared, and 100 μL of each dilution was spread onto the surface of sterile nutrient agar plates. Total aerobic counts were enumerated on plate count agar (PCA) and incubated at 30 °C for 48 h. Coliforms were enumerated on Violet Red Bile Lactose agar (VRBL), with incubation for 24 h at 37 or 44 °C for total and fecal coliforms, respectively. Psychrophilic bacteria were assessed using PCA after incubation at 4 °C for 5 days. The presence of *Salmonella* was determined through a presence-absence test. Initially, 25 g samples were homogenized in 225 mL of buffered peptone water and incubated for 24 h at 37 °C. After incubation, 1 mL was transferred to 10 mL of selenite–cystine broth and incubated at 37 °C for 24 h. Subsequently, a loopful of broth was plated onto Hektoen medium and incubated at 37 °C for 24 h. The bacterial numbers were converted to log10 colony-forming units per gram (CFU g^{-1}).

2.15. Inductively coupled plasma analysis

The concentration of attached Ag to CNCs, as well as the amount of Ag released from CNCs-AgNPs, PVA/CNCs-AgNPs, and chicken breast fillet films, was measured using

inductively coupled plasma atomic emission spectrometry (ICP-AES) with a PerkinElmer OPTIMA 3000 instrument. A weighed portion of CNCs-AgNPs film (about 150 mg) was digested in 5 mL of 80% nitric acid until the film was fully dissolved. Water (10 mL) was added, and the mixture was refluxed for 3 h to ensure a complete breakdown of cellulose and full mineralization of Ag.

3 Results and discussion

3.1. Ox-CNCs-AgNPs characterization

Immediately after the addition of Tollens' reagent $[Ag(NH_3)_2]^+$ to the ox-CNCs suspension, a color change from transparent to brownish occurred within 5 min, turning more brown with time, and the color was stable within 30 min. The rapid change in the suspension color suggested that the entire process, encompassing reduction, nucleation, and AgNP formation occurred spontaneously and rapidly, implying that increasing temperature or introducing an external reducing agent to facilitate the process was unnecessary. This color evolution was accompanied by the emergence of a strong absorption peak at 420 nm in the UV-Vis spectrum of the suspension, which is the typical signature of AgNPs reflecting their surface plasmon resonance (SPR) (Fig. 1A).[39] Interestingly, the color evolution of the suspension was not accompanied by particle sedimentation, and the suspension remained colloidally stable. This was further confirmed by measuring the particle size and ζ-potential of the suspensions before and after formation of AgNPs. As illustrated in Fig. 1B, the introduction of $[Ag(NH_3)_2]^+$ caused a noticeable shift in the particle size distribution, increasing the equivalent diameter of particles from 168 nm for ox-CNCs to 245 nm for CNCs-AgNPs. Despite this increase in size, the ζ-potential remained negative after periodate oxidation and the addition of $[Ag(NH_3)_2]^+$ (−35.7 mV and −30.8 mV, respectively), providing electrostatic repulsion and ensuring colloidal stability.

As shown by the TEM images of Fig. 2A, the neat CNCs displayed the typical rodlike morphology with an average length of 150 nm. After treatment of the ox-CNCs with Tollens' reagent, black dots appeared on their surface, corresponding to newly-formed AgNPs (Fig. 2B and C). However, three observations can be made: (i) the generated AgNPs were polydisperse with a size ranging from 3 to 20 nm; (ii) the functionalization of CNCs by AgNPs was heterogeneous since a fraction of CNCs was devoid of visible AgNPs; (iii) The AgNPs appeared to be attached to the CNCs, and no free NPs were observed. This agreed with our previous work using periodate-oxidized CNFs instead of CNCs,[23] and was explained by the specificity of the aldehyde function of ox-CNCs as reducing entity for the $[Ag(NH_3)_2]^+$ precursor, and the mechanism of Ag^0 formation that favors the binding of Ag^0 onto the CNC surface. We assumed that the lack of AgNPs on a fraction of CNCs was due to a significant fraction of aldehyde groups being converted to hemiacetal, which could not reduce $[Ag(NH_3)_2]^+$. However, other explanations cannot be excluded, and further work is needed to resolve this issue.

The XRD analysis of a CNCs-AgNPs film helped identify the chemical nature of the nanoparticles (Fig. 3A). In addition to the diffraction peaks of ox-CNCs at 2θ = 16.2, 22.4, and 34.8° attributed to cellulose I, the XRD profile of CNCs-AgNPs exhibited peaks at 38.2 and 44.4°.[23,39] These corresponded to the (111) and (200) planes of the face-centered cubic structure of metallic Ag (JCPDS file no. 87-0720) and not to Ag_2O, since the peak at 44.4° is specific to Ag.[40] In addition, applying Scherrer's equation to the width at half-height of the Ag diffraction peaks provided a particle size of 12 nm, in good agreement with the average size of 14 nm determined from the TEM images (Fig. S1†).

The thermal stability of ox-CNCs and CNCs-AgNPs was assessed by TGA (Fig. 3B). The thermogram of ox-CNCs displayed an initial weight loss of about 10% at around 90 °C due to moisture removal, followed by a steep loss starting at 150 °C and extending up to 500 °C attributed to the thermal degradation of the cellulose backbone. For CNCs-AgNPs, the weight loss due to moisture sorption was lower (around 2%), and the onset of thermal degradation occurred at around 180 °C, with a two-step loss occurring at 200 and 450 °C, respectively. The lower thermal stability of ox-CNCs was reported in the literature and attributed to the presence of aldehyde groups that are more

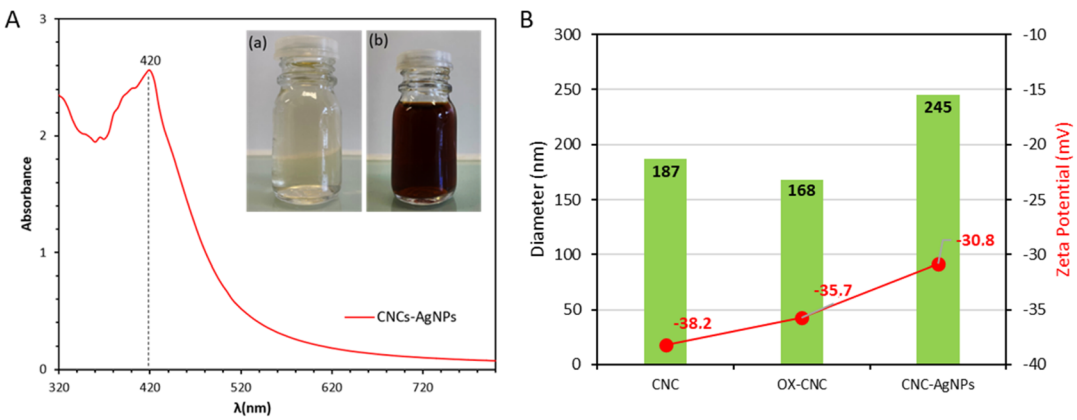

Fig. 1 (A) Electronic absorption spectra of a CNCs-AgNPs suspension in water. Inset images: photographs of ox-CNCs (a) and CNCs-AgNPs (b) suspensions; (B) average particle size and zeta potential of CNCs, ox-CNCs, and CNCs-AgNPs.

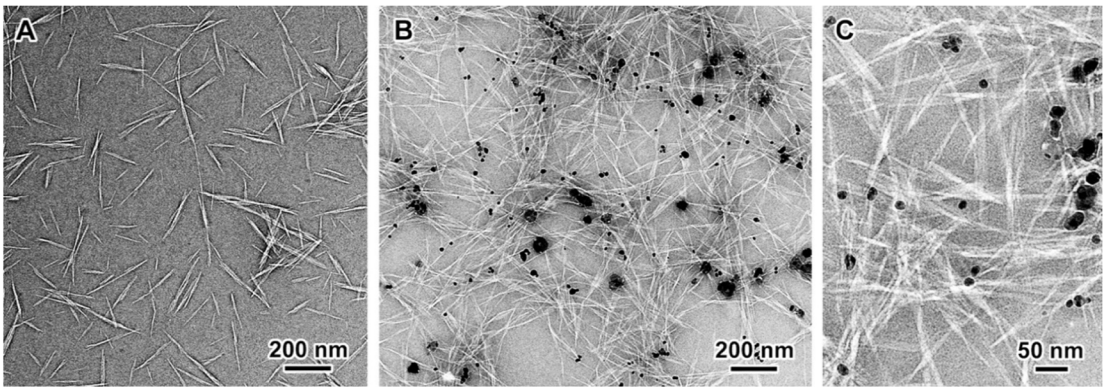

Fig. 2 TEM images of negatively stained preparations form suspensions of initial CNCs (A) and CNCs-AgNPs (B and C). The AgNPs appear as black dots.

prone to thermal decomposition than the hydroxyl groups.[41] The shift to a higher temperature for CNCs-AgNPs was presumably due to the consumption of aldehyde groups after the reaction with the $[Ag(NH_3)_2]^+$ precursor, the ash content of CNCs-AgNPs was about 20%, which was significantly higher than that of ox-CNC (around 10%), indicating a high content of metallic Ag in CNCs-AgNPs.

3.2. Antibacterial activity of CNCs-AgNPs

To assess the antibacterial efficacy of CNCs/AgNPs at concentrations of 10, 20, and 40 mg mL^{-1}, eight pathogenic bacteria, namely four Gram– (*E. coli*, *K. pneumoniae*, *P. aeruginosa*, *S. enterica*) and four Gram+ (*S. aureus*, *M. luteus*, *L. monocytogenes*, *E. faecalis*) bacteria, were subjected to the agar well diffusion method (Fig. S2†). The antibacterial activity was determined by measuring the diameter of the growth inhibition zone and calculating the minimum inhibitory concentration (MIC) values (Table 1), with ampicillin serving as a positive control. The antibacterial activity intensified with increasing AgNP concentration. The largest regions of inhibition (15 to 20 mm) were observed for 40 mg mL^{-1} CNCs-AgNPs against both Gram+ and Gram– bacteria. Particularly sensitive strains included *S. aureus*, *M. luteus*, *E. faecalis*, and *S. enterica*, exhibiting inhibition regions with diameters of 18, 18, 20, and 20 mm, respectively. Panáček *et al.* reported that the attachment of Ag species to a microorganism cell membrane resulted in a profound disturbance in vital functions, including permeability, respiration, and replication.[42] Although the precise mechanism of AgNP antibacterial action remains unclear, it was postulated that AgNPs interact with the outer bacterial membrane, inducing structural changes and membrane degradation that result in cell death. In addition, strains with larger inhibition regions exhibited lower MIC values (Table 1), representing the minimum CNCs-AgNPs concentration completely inhibiting strain growth after 24 h of incubation. Regardless of bacterial species, CNCs-AgNPs at concentrations corresponding to the MIC reduced cell populations after 24 h of incubation. The MIC values indicated that CNCs-AgNPs effectively inhibited the growth of Gram+ and Gram– bacteria within a concentration range of 0.8 to 3.2 mg mL^{-1}. Notably, CNCs-AgNPs demonstrated strong inhibitory effects against *M. luteus* and *E. faecalis*, with a low MIC *ca.* 0.8 mg mL^{-1}.

3.3. Determination of antibacterial activity of CNCs-AgNPs

The growth of foodborne pathogenic bacteria in liquid broth was assessed at a concentration of CNCs-AgNPs ranging from

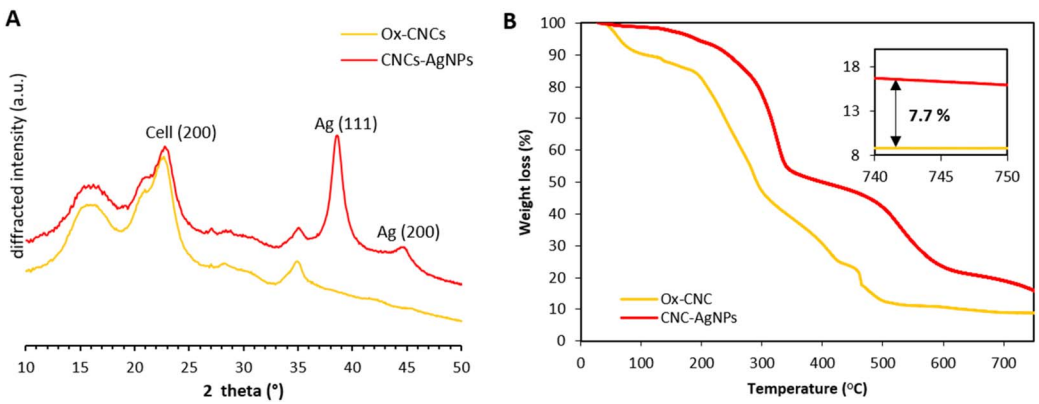

Fig. 3 (A) XRD profiles of ox-CNCs (orange) and CNCs-AgNPs (red); (B) TGA thermograms for ox-CNCs (orange), and CNCs-AgNPs (red).

Table 1 Region of inhibition (mm) and MIC (mg mL^{-1}) for Gram+ and Gram− bacterial strains in the presence of different CNCs-AgNPs concentrations; NI: no inhibition; control: ampicillin (25 μg mL^{-1} for all tested bacteria)

	Control	CNCs-AgNPs (mg mL^{-1})/region of inhibition diameter (mm)			MIC (mg mL^{-1})
Bacterial strains	25 (μg mL^{-1})	10	20	40	CNCs-AgNPs
Gram + bacteria					
S. aureus	NI	13 ± 0.55	15 ± 0.42	18 ± 0.25	1.6
L. monocytogenes	25 ± 0.25	11 ± 0.31	13 ± 0.37	15 ± 0.36	3.2
M. luteus	26 ± 0.45	12 ± 0.42	15 ± 0.35	18 ± 0.41	0.8
E. faecalis	24 ± 0.66	14 ± 0.52	15 ± 0.25	20 ± 0.50	0.8
Gram− bacteria					
E. coli	30 ± 0.45	11 ± 0.22	14 ± 0.54	16 ± 0.70	3.2
P. aeruginosa	NI	10 ± 0.41	11 ± 0.66	16 ± 0.65	1.6
S. enterica	2 7 ± 0.35	13 ± 0.33	15 ± 0.23	20 ± 0.25	1.6
K. pneumoniae	25 ± 0.30	12 ± 0.40	13 ± 0.19	16 ± 0.55	3.2

0.1 to 6.4 mg mL^{-1} (Fig. 4). The quantification of viable CFU of foodborne pathogenic bacteria on agar plates was conducted after an 18 h incubation period (Fig. S3†). A notable antibacterial efficiency of CNCs-AgNPs was observed, with the incorporation of CNCs-AgNPs impacting growth compared to the control without CNCs-AgNPs. The bacterial strain growth was partially inhibited at 0.2 mg mL^{-1} of CNCs-AgNPs. Beyond 3.2 mg mL^{-1}, no bacterial growth was observed for all tested foodborne strains, and the CFU count decreased with increasing CNCs-AgNPs concentration, resulting in total cell destruction. CNCs-AgNPs inhibited the bacterial growth of *P. aeruginosa*, *S. enterica*, and *S. aureus* at 1.6 mg mL^{-1}. In addition, *E. coli*, *L. monocytogenes*, and *K. pneumoniae* were inhibited at 3.2 mg mL^{-1}. *M. luteus* and *E. faecalis* proved to be the most sensitive strains, being completely inhibited at 0.8 mg mL^{-1} CNCs-AgNPs. Conversely, the control culture exhibited numerous bacterial colonies on the agar plates.

The antibacterial activity of various cellulose-AgNPs systems has previously been demonstrated by other authors. Lokanathan *et al.* previously showed that CNCs-AgNPs composites, prepared in the presence of borohydride as reducing agent, could effectively achieve complete inhibition of *S. aureus* growth over 72 h.[5] Sofi *et al.* described the preparation of CNF mats incorporating both hydroxyapatite (HAp) and AgNPs, exhibiting exceptional antibacterial properties against *S. aureus* and *E. coli.*[43] The most potent antibacterial performance was observed in mats containing 1.5 wt% HAp and 7 wt% AgNPs, which achieved a maximum zone of inhibition of 2.79 ± 0.23 mm against *E. coli* and 1.64 ± 0.33 mm against *S. aureus*.

3.4. Characterization of PVA and PLLA films incorporating CNCs-AgNPs

3.4.1. Mechanical properties. CNCs-AgNPs can be potentially used as active nanofiller in a thin polymer film, where the

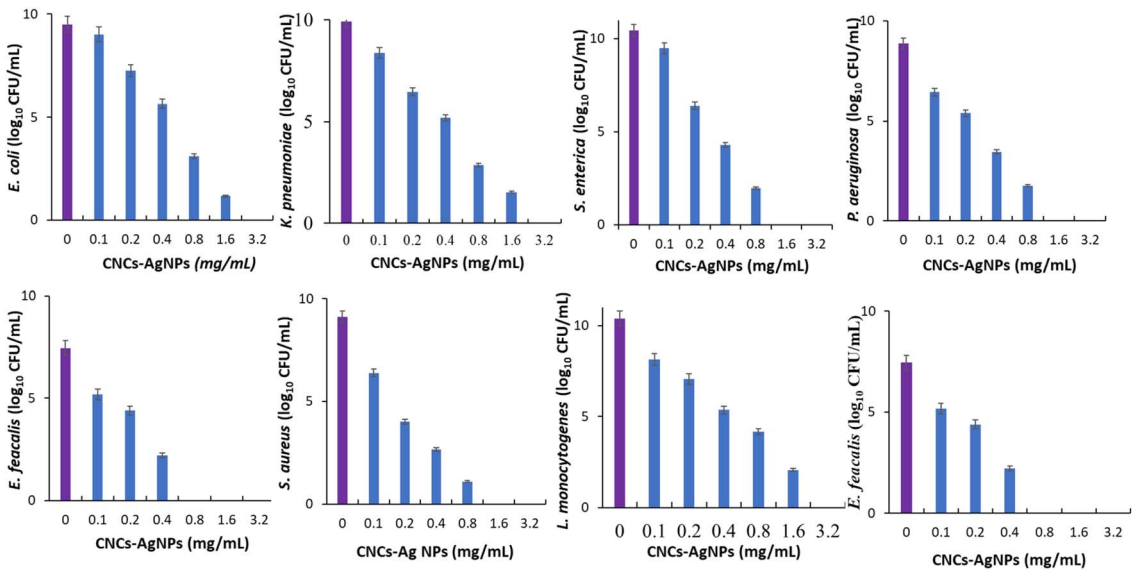

Fig. 4 The antimicrobial activity of different concentrations of CNCs-AgNPs against Gram+ and Gram− bacteria by colony-forming unit technique.

CNC would contribute to enhancing the mechanical properties of the polymer thanks to the strong reinforcing aptitude of CNCs, while the AgNPs would provide a bactericidal effect. For this purpose, thin films incorporating different CNCs-AgNPs contents were prepared, and their mechanical properties were investigated. The effect of adding CNCs-AgNPs up to 4 wt% on the mechanical properties of the PVA and PLLA-PEG films was studied by tensile test analysis. The stress–strain plot for PVA and PLLA-PEG for neat films and at 2 and 4 wt% CNCs-AgNPs is presented in Fig. 5. The inclusion of CNCs-AgNPs markedly increased the tensile strength (σ) and modulus (E) of both types of films, which means that the presence of AgNPs attached to CNCs did not compromise their reinforcing potential. However, the reinforcement was much more significant for the PVA matrix than PLLA-PEG. Indeed, at 2 and 4 wt% CNCs-AgNPs, the increment in σ reached 84 and 154%, respectively, while it was only 37 and 17% for the PLLA-PEG matrix. With the incorporation of 4 wt% CNCs-AgNPs, the modulus of PVA and PLLA films significantly increased by 25 and 75%, respectively, compared to their neat matrices. However, the incorporation of rigid CNC-AgNPs reduced the overall flexibility of both PLLA and PVA matrices and resulted in a lower elongation at break. This was attributed to the increased rigidity of the films, a typical behavior of composites into which NC was added.[44] Beyond its role as dispersing agent, PEG also acted as a plasticizer, markedly reducing the stiffness of neat PLLA (data not shown) by lowering its ultimate stress and elastic modulus, respectively, in agreement with our previous works.[45,46]

One reason for this difference in the mechanical behavior of the films with PVA and PLLA matrices would be the better nanofiller dispersion in the hydrophilic PVA compared to the hydrophobic PLLA, allowing to take better advantage of the reinforcing effect which is known to take place *via* the set-up of a percolated network among the rigid CNCs. On the other hand, in PLLA matrices, even though PEG was used as a carrier to facilitate the dispersion of CNCs in the PLLA matrix, aggregation was likely to inevitably occur, especially with increasing CNC content. This result was also observed in our previous works regarding the effect of the inclusion of CNCs in PLLA using PEG as a carrier.[45,46] Overall, the mechanical performance of the films meets the requirement for food packaging, where a balance between tensile strength and flexibility is essential to withstand the mechanical stresses of handling and transportation.[47]

3.4.2. Antibacterial activity of PVA/CNCs-AgNPs and PLLA/CNCs-AgNPs nanocomposite films. To demonstrate the antibacterial effectiveness of CNCs-AgNPs when incorporated in a polymer matrix, a diffusion test was conducted for PVA and PLLA films containing 2 and 4 wt% of CNCs-AgNPs. The results presented in Table S1† showed that the antimicrobial activity of PVA/CNCs-AgNPs and PLLA/CNCs-AgNPs films increased with higher CNCs-AgNPs content in both PVA and PLLA films. PVA/CNCs-AgNPs (4 wt%) films exhibited larger inhibition regions against all tested bacteria compared to PLLA/CNCs-AgNPs (4 wt%) films. This indicates that the strong antibacterial action of CNCs-AgNPs was preserved even when incorporated

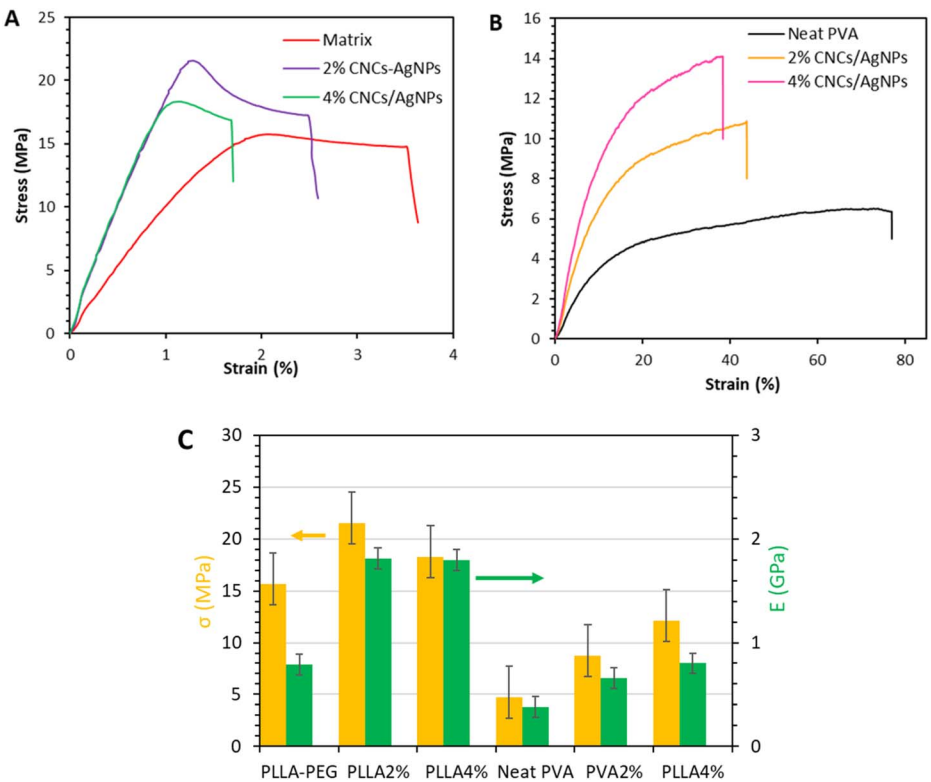

Fig. 5 Stress–strain curves of PLLA-PEG (A) and PVA (B) films with different CNCs-AgNPs contents; (C) corresponding strength σ and modulus E.

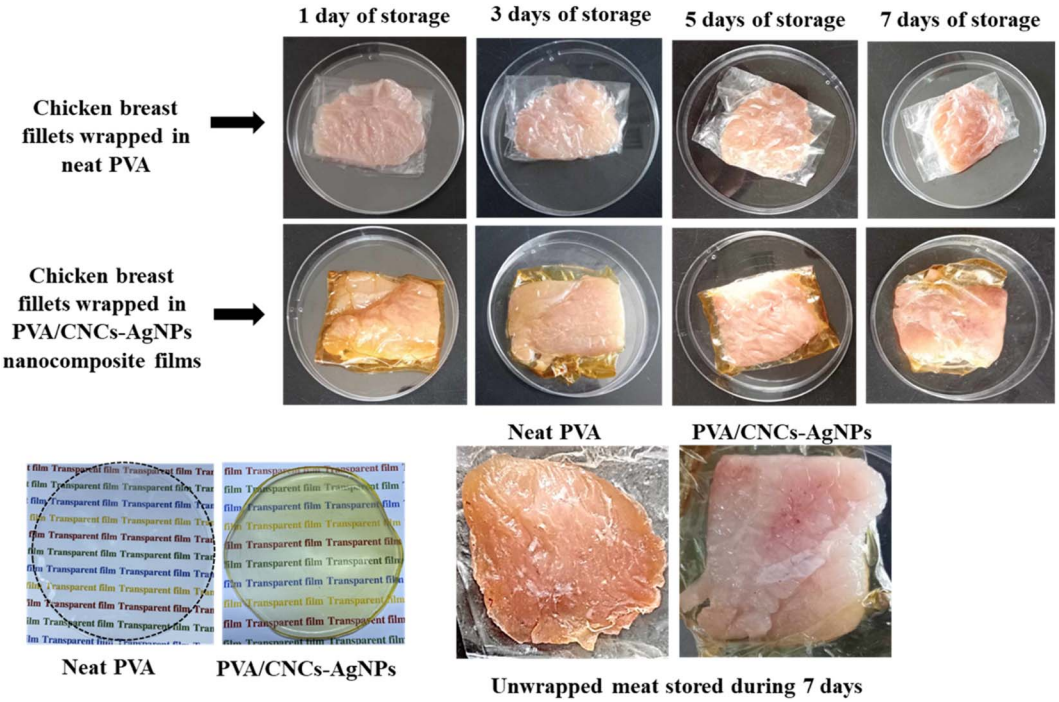

Fig. 6 Chicken meat pieces wrapped in PVA/CNCs-AgNPs nanocomposite films placed inside sterile bags and stored at 4 °C.

into polymer matrices, and this antibacterial effect could be modulated by the CNCs-AgNPs content. Interestingly, PVA films exhibited significant antimicrobial activity against various bacterial strains, including Gram+ *S. aureus*, *M. luteus*, and *E. feacalis*, as well as Gram– *E. coli*, *S. enterica*, and *K. pneumoniae*. However, neat PVA and PLLA films showed no antibacterial effect against the tested foodborne pathogenic bacterial strains. The antibacterial performance was primarily attributed to the presence of CNCs-AgNPs in the nanocomposites.

In the context of packaging films containing AgNPs, Ag is inevitably released from the material due to diffusion from the AgNPs. It was thus imperative to assess the extent of Ag migration in PVA films containing 2 and 4 wt% CNCs-AgNPs after immersion in 3% acetic acid simulating food contact conditions. The amount of released Ag after 6, 24, and 48 h was quantified using inductively coupled plasma (ICP) analysis. Surprisingly, the amount of released Ag was below 0.02 mg L^{-1} for all samples, in line with the migration limit set by the European Food Safety Authority at 0.05 mg^{-1}. The low amount of Ag released from the PVA/CNC-AgNPs film was attributed to the effective binding of AgNPs to CNCs. This absence of migration or diffusion of AgNPs from the PVA/CNC-AgNPs films offers significant advantages, especially for applications in food packaging using fully hydrolyzed PVA films. This highlights the crucial role of using dialdehyde-functionalized CNCs as reducing agents for the formation of AgNPs, ensuring strong binding with CNCs while enhancing the mechanical properties of the composite material.

3.4.3. Evaluation of PVA/CNCs-AgNPs films for chicken breast fillet packaging. As a proof of concept to demonstrate the practical usefulness of CNCs-AgNPs as an additive for active packaging, a thin, flexible PVA film with a thickness of approximately 100 μm containing 4 wt% CNCs-AgNPs was prepared by casting. Chicken breast fillets were wrapped with either a control film (neat PVA) or a PVA film containing 4 wt% CNCs-AgNPs under refrigerated storage and the microbial flora was counted at different intervals (Fig. 6). The initial values for total viable counts and psychrophilic bacteria were 3.5 log and 2.8 log CFU g^{-1}, respectively, indicating that the chicken breast fillets had good microbiological quality. Table S2† illustrates the variations in total viable counts, psychrophilic bacteria, total and fecal coliforms, and *Salmonella* in chicken breast fillets.

Throughout refrigerated storage, regardless of the packaging material used, bacterial growth increased over time. The PVA films incorporating CNCs-AgNPs exhibited significant inhibitory effects ($p < 0.05$) against bacteria compared to the control film (neat PVA). The total number of viable bacteria was significantly reduced ($p < 0.05$) up to day 7 from 6.1 log CFU g^{-1} to 5.58 log CFU g^{-1} when chicken breast fillets were wrapped with nanocomposite films compared to control films. According to Azlin-Hasim *et al.*, the acceptable limit for the total viable count of chicken breast fillet products is 6 log CFU g^{-1}.[48] In addition, following the Commission Regulation No 1441/2007 (EC, 2007), the acceptable limit for the total viable count of chicken meat products ranges from 6 to 7 log CFU g^{-1}. In this study, chicken breast fillets wrapped in control films reached their acceptability limit by day 7. In contrast, the shelf life of chicken breast fillets wrapped in antimicrobial PVA/CNCs-AgNPs nanocomposite films surpassed the 7 day mark. Furthermore, upon reaching the end of the shelf life (day 7), notable suppression of psychrophilic bacteria, total coliforms,

and fecal coliforms was observed in chicken breast fillets covered with nanocomposite films, registering values of 4.85, 2.87, and 2.25 log CFU g^{-1}, respectively *versus* 5.54, 3.45 and 3.0 log CFU g^{-1}, determined in chicken breast fillets wrapped in PVA films.

The amount of migrated Ag in chicken meat was evaluated by ICP analysis after mineralization of dried chicken samples. The level of residual Ag after 10 days in contact with the wrapping film was *ca.* 0.035 mg kg^{-1} of meat, which was lower than the threshold value recommended by the European Food Safety Authority for various Ag-based substances intended for food contact and with a specific migration limit of 0.05 mg Ag per kg of food.[49] This limit serves as a regulatory standard to ensure the safety of food when in contact with such materials.

4 Conclusions

In this study, periodate-oxidized CNCs were successfully decorated with AgNPs, and the antibacterial properties of CNCs-AgNPs nanocomposites in PVA and PLLA matrices were evaluated. The concentration-dependent antibacterial activity of CNCs-AgNPs against various foodborne pathogens was confirmed by agar well diffusion and MIC assays, emphasizing their bactericidal efficacy. The mechanical properties of PVA and PLLA films were significantly improved by incorporating 2 wt% CNCs-AgNPs, as reflected by an enhanced tensile strength due to strong intermolecular interactions and the load-bearing capacity of CNCs. Although the use of PEG as a plasticizer reduced the tensile strength of PLLA films, CNCs-AgNPs counteracted this effect, reinforcing the overall mechanical performance. Practical applications were demonstrated by wrapping chicken breast fillets in PVA/CNCs-AgNPs nanocomposite films, which effectively inhibited bacterial growth and extended the shelf life of the meat beyond microbiological safety limits. These results highlight the dual functionality of CNCs-AgNPs nanocomposites as antibacterial agents and mechanical reinforcements, paving the way for innovative and sustainable food packaging solutions. Future work could further explore the long-term stability of these nanocomposites under real storage conditions, as well as their behavior in contact with different food matrices.

Data availability

Data associated with this study have not been deposited into a publicly available repository. Data will be made available on request.

Author contributions

Mohamed Aouay: writing – original draft, investigation, formal analysis, writing – review & editing. Anissa Haddar: conceptualization, writing – review & editing. Emna Sallemi: writing – original draft, investigation, formal analysis. Albert Magnin: project administration, funding acquisition, writing – review & editing. Jean-Luc Putaux: investigation, writing – review & editing. Sami Boufi: project administration, conceptualization, funding acquisition, writing – review & editing.

Conflicts of interest

The authors declare no conflict of interest.

Acknowledgements

The authors acknowledge Partenariat Hubert Curien (CMCU project: 23G1118), LabEx Tec21 (Investissements d'Avenir #ANR-11-LABX-0030), and the Glyco@Alps programme (Investissements d'Avenir #ANR-15-IDEX-02) for financial support. We thank the NanoBio-ICMG Platform (UAR 2607, Grenoble) for granting access to the Electron Microscopy facility. CERMAV and LRP are part of Institut Carnot PolyNat (Investissements d'Avenir #ANR-11-CARN-030-01).

References

1 N. Mahfoudhi and S. Boufi, *Cellulose*, 2017, **24**, 1171–1197.
2 A. Dufresne, *Mater. Today*, 2013, **16**, 220–227.
3 D. Klemm, F. Kramer, S. Moritz, T. Lindström, M. Ankerfors, D. Gray and A. Dorris, *Angew. Chem., Int. Ed.*, 2011, **50**, 5438–5466.
4 F. Wang, Z. Hu, S. Ouyang, S. Wang, Y. Liu, M. Li, Y. Wu, Z. Li, J. Qian, Z. Wu, Z. Zhao, L. Wang, C. Jia and S. Ma, *Int. J. Biol. Macromol.*, 2024, **268**, 131936.
5 A. R. Lokanathan, K. M. A. Uddin, O. J. Rojas and J. Laine, *Biomacromolecules*, 2014, **15**, 373–379.
6 S. Y. H. Abdalkarim, L.-M. Chen, H.-Y. Yu, F. Li, X. Chen, Y. Zhou and K. C. Tam, *Int. J. Biol. Macromol.*, 2021, **182**, 1915–1930.
7 S. Y. H. Abdalkarim, L.-M. Chen, H.-Y. Yu, F. Li, X. Chen, Y. Zhou and K. C. Tam, *Int. J. Biol. Macromol.*, 2021, **182**, 1915–1930.
8 Q. Zhang, L. Zhang, W. Wu and H. Xiao, *Carbohydr. Polym.*, 2020, **229**, 115454.
9 L. Heath and W. Thielemans, *Green Chem.*, 2010, **12**, 1448–1453.
10 A. R. Deshmukh, P. K. Dikshit and B. S. Kim, *Int. J. Biol. Macromol.*, 2022, **205**, 169–177.
11 M. A. Khalilzadeh, S. Tajik, H. Beitollahi and R. A. Venditti, *Ind. Eng. Chem. Res.*, 2020, **59**, 4219–4228.
12 M. S. Islam, L. Chen, J. Sisler and K. C. Tam, *J. Mater. Chem. B*, 2018, **6**, 864–883.
13 F. Awan, M. S. Islam, Y. Ma, C. Yang, Z. Shi, R. M. Berry and K. C. Tam, *ACS Omega*, 2018, **3**, 12403–12411.
14 P. Xu, C. Cen, N. Chen, H. Lin, Q. Wang, N. Xu, J. Tang and Z. Teng, *J. Colloid Interface Sci.*, 2018, **526**, 194–200.
15 X. Wang, J. Guo, H. Ren, J. Jin, H. He, P. Jin, Z. Wu and Y. Zheng, *Trends Food Sci. Technol.*, 2024, **143**, 104289.
16 M. Ö. Seydibeyoğlu, A. Dogru, J. Wang, M. Rencheck, Y. Han, L. Wang, E. A. Seydibeyoğlu, X. Zhao, K. Ong, J. A. Shatkin, S. Shams Es-haghi, S. Bhandari, S. Ozcan and D. J. Gardner, *Polymers*, 2023, **15**, 984.

17 J. Lv, X. Zhang, N. Yu, S. Su, J. Zhu, L. Deng and Z. Liu, *Cellulose*, 2019, **26**, 7837–7846.
18 K. M. A. Uddin, A. R. Lokanathan, A. Liljeström, X. Chen, O. J. Rojas and J. Laine, *Green Mater.*, 2014, **2**, 183–192.
19 Z. Shi, J. Tang, L. Chen, C. Yan, S. Tanvir, W. A. Anderson, R. M. Berry and K. C. Tam, *J. Mater. Chem. B*, 2014, **3**, 603–611.
20 Y. He, H. Li, X. Fei and L. Peng, *Carbohydr. Polym.*, 2021, **252**, 117156.
21 H. Yu, B. Sun, D. Zhang, G. Chen, X. Yang and J. Yao, *J. Mater. Chem. B*, 2014, **2**, 8479–8489.
22 H. Liu, J. Song, S. Shang, Z. Song and D. Wang, *ACS Appl. Mater. Interfaces*, 2012, **4**, 2413–2419.
23 A. Errokh, A. Magnin, J.-L. Putaux and S. Boufi, *Mater. Sci. Eng. C*, 2019, **105**, 110044.
24 S. Mangaraj, A. Yadav, L. M. Bal, S. K. Dash, N. K. Mahanti and J. Packag, *Technol. Res.*, 2019, **3**, 77–96.
25 E. Fortunati, M. Peltzer, I. Armentano, L. Torre, A. Jiménez and J. M. Kenny, *Carbohydr. Polym.*, 2012, **90**, 948–956.
26 E. Fortunati, S. Rinaldi, M. Peltzer, N. Bloise, L. Visai, I. Armentano, A. Jiménez, L. Latterini and J. M. Kenny, *Carbohydr. Polym.*, 2014, **101**, 1122–1133.
27 E. Fortunati, M. Peltzer, I. Armentano, A. Jiménez and J. M. Kenny, *J. Food Eng.*, 2013, **118**, 117–124.
28 H. Zhang, H.-Y. Yu, C. Wang and J. Yao, *Carbohydr. Polym.*, 2017, **173**, 7–16.
29 E. Fortunati, F. Luzi, D. Puglia, A. Terenzi, M. Vercellino, L. Visai, C. Santulli, L. Torre and J. M. Kenny, *Carbohydr. Polym.*, 2013, **97**, 837–848.
30 X. Chen, B. Xiao, Y. Yang, Y. Jiang, X. Song, F. Chen, W. Wang, J. Wu and Y. Meng, *Prog. Org. Coat.*, 2024, **186**, 108042.
31 M. Julinová, L. Vaňharová and M. Jurča, *J. Environ. Manage.*, 2018, **228**, 213–222.
32 Q. Zhang, M. Song, Y. Xu, W. Wang, Z. Wang and L. Zhang, *Prog. Polym. Sci.*, 2021, **120**, 101430.
33 E. E. Yalcinkaya, D. Puglia, E. Fortunati, F. Bertoglio, G. Bruni, L. Visai and J. M. Kenny, *Carbohydr. Polym.*, 2017, **157**, 1557–1567.
34 S. Hajji, R. B. S.-B. Salem, M. Hamdi, K. Jellouli, W. Ayadi, M. Nasri and S. Boufi, *Process Saf. Environ. Prot.*, 2017, **111**, 112–121.
35 P. Ma, L. Jiang, M. Yu, W. Dong and M. Chen, *ACS Sustain. Chem. Eng.*, 2016, **4**, 6417–6426.
36 L. Fan, H. Zhang, M. Gao, M. Zhang, P. Liu and X. Liu, *Holzforschung*, 2020, **74**, 523–528.
37 M. S. Sarwar, M. B. K. Niazi, Z. Jahan, T. Ahmad and A. Hussain, *Carbohydr. Polym.*, 2018, **184**, 453–464.
38 J. M. Andrews, *J. Antimicrob. Chemother.*, 2001, **48**, 5–16.
39 C. Noguez, *J. Phys. Chem. C*, 2007, **111**, 3806–3819.
40 A. M. Awwad, N. M. Salem and A. O. Abdeen, *Int. J. Ind. Chem.*, 2013, **4**, 29.
41 U.-J. Kim and S. Kuga, *Thermochim. Acta*, 2001, **369**, 79–85.
42 A. Panáček, M. Kolář, R. Večeřová, R. Prucek, J. Soukupová, V. Kryštof, P. Hamal, R. Zbořil and L. Kvítek, *Biomaterials*, 2009, **30**, 6333–6340.
43 H. S. Sofi, T. Akram, N. Shabir, R. Vasita, A. H. Jadhav and F. A. Sheikh, *Mater. Sci. Eng. C*, 2021, **118**, 111547.
44 A. Najahi, Q. Tarrés, P. Mutjé, M. Delgado-Aguilar, J.-L. Putaux and S. Boufi, *Nanomaterials*, 2023, **13**, 126.
45 M. Aouay, A. Magnin, J.-L. Putaux and S. Boufi, *Ind. Crops Prod.*, 2023, **202**, 117011.
46 M. Aouay, A. Magnin, J.-L. Putaux and S. Boufi, *Int. J. Biol. Macromol.*, 2022, **218**, 588–600.
47 J. Cheng, R. Gao, Y. Zhu and Q. Lin, *Alex. Eng. J.*, 2024, **91**, 70–83.
48 S. Azlin-Hasim, M. C. Cruz-Romero, M. A. Morris, E. Cummins and J. P. Kerry, *Food Packag. Shelf Life*, 2015, **4**, 26–35.
49 European Commission Regulation, *European Commission Regulation (EU) No 10/2011 of 14 January 2011 on plastic materials and articles intended to come into contact with food*, 2011, **https://eur-lex.europa.eu/eli/reg/2011/10/2025-01-20**.